Skeletonization: An Electrostatic Field-Based Approach [1]

Tanya Grigorishin, Gamal Abdel-Hamid[2], and Yee-Hong Yang[3]

Computer Vision Laboratory,
Department of Computer Science
University of Saskatchewan,
Saskatoon, Saskatchewan,
Canada S7N 5A9

Email Address for Y.H. Yang: yang@cs.usask.ca
Phone Number for Y.H. Yang: (306) 966-4891
Fax Number for Y.H. Yang: (306) 966-4884

February 1, 1996

ABSTRACT

Skeleton representation of an object is a powerful shape descriptor that captures both boundary and region information of the object. The skeleton of a shape is a representation composed of idealized thin lines that preserve the connectivity or topology of the original shape. Although the literature contains a large number of skeletonization algorithms, many open problems remain.

In this paper, we present a new skeletonization approach that relies on the Electrostatic Field Theory (EFT). Many problems associated with existing skeletonization algorithms are solved using the proposed approach. In particular, connectivity, thinness, and other desirable features of a skeleton are guaranteed. It also captures notions of corner detection, multiple scale, thinning, and skeletonization all within one unified framework.

The performance of the proposed EFT-based algorithm is studied extensively. Using the Hausdorf distance measure, the noise sensitivity of the algorithm is compared to two existing skeletonization techniques. The experimental results are encouraging.

[1] The authors would like to acknowledge financial support provided by NSERC through grant number OGP0000370.

[2] Gamal Abdel-Hamid passed away on Dec. 4, 1994

[3] To whom correspondence should be addressed. Grigorishin and Yang would like to dedicate this paper in memory of Abdel-Hamid.

1 Introduction

Shape representation and description plays an important role in most computer vision systems. A useful and reliable shape representation must meet a number of requirements, which include *invariance*, *uniqueness*, and *stability* [1, 2]. If two objects have the same shape, then their representations should be the same and should be invariant with respect to translation, rotation, and scaling. Uniqueness means that if two objects have different shapes they should have different representations. Stability denotes the fact that if two objects have a small shape difference, then their representations should have a small difference. Conversely, if two representations have a small difference, then the objects they represent should also have a small shape difference. Therefore, a stable representation means a representation that is insensitive to noise. In short, the object shape and its representation should have a one-to-one correspondence property.

The representation should reflect the shape of an object at various levels of abstraction and should also combine both boundary and region information of the object. Finally, the shape descriptors and the recognition of objects should be efficiently computable. Other criteria for shape representation can be found in reference [2].

The skeleton of a two-dimensional object is a transformation which maps the contour of the object into a one-dimensional line. Skeleton representation as introduced by Blum [3] meets most of the aforementioned requirements.

Since the introduction of the skeleton shape descriptor, many skeletonization algorithms have been reported in the literature [4]. Many problems, however, remain unsolved. For example, methods to quantitatively evaluate skeletons are still lacking. Recently, there are some efforts done in this direction [6, 7, 8, 9]. The philosophy of performance analysis, pointing to the lack of

performance evaluation in image analysis algorithms, is also discussed in [5].

Another problem with most skeletonization algorithms is their sensitivity to noise. Although there are many skeletonization algorithms, surprisingly little work has been directed towards studying their sensitivity to boundary noise. Also, some existing skeletonization approaches require that many parameters be supplied by the user [10].

In this paper, a new skeletonization approach based on the Electrostatic Field Theory (EFT) for shapes with no holes is proposed. The motivation of this research work stems from the following reasons. First, the encouraging results of a recently developed corner detector based on the same underlying theory, the EFT [11], suggest the possibility of applying the EFT to determine skeletons. In reference [11] it was pointed out that electrostatic field lines represent lines of symmetry naturally. Secondly, EFT presents a natural solution for skeletonization which can overcome many of the difficulties of existing approaches, such as connectivity and noise sensitivity. Thirdly, EFT unifies notions of corner detection, thinning, skeletonization, and multiple scale representation of objects, all within the same framework.

The paper is organized as follows. An overview of the related research is discussed in Section 2. The proposed approach for skeletonization is presented in Section 3. The experimental results obtained and the analysis of the EFT-based approach are presented in Section 4. Section 5 describes the performance characterization experiments and the experimental comparison between the proposed approach, a distance transform based approach [24] and the Charge Particle Method for skeletonization [27]. Finally, conclusions and future directions are discussed in Section 6.

2 Related Work

This section gives a brief review of skeletonization algorithms along with their main characteristics and drawbacks. For a more complete survey of skeletonization algorithms the interested reader can consult reference [4].

Existing skeletonization approaches can be classified approximately into a small number of categories. The first category is based on *topological* or *direct thinning*. Thinning denotes the process of iteratively peeling away the object's contour pixels while preserving its topology [13]. Many thinning techniques have been developed, including both sequential [14] and parallel [15] algorithms. The drawbacks of thinning algorithms are noise sensitivity, loss of continuity, and distortion, which usually lead to counterintuitive results. Therefore, most thinning approaches have been directed towards character recognition applications. The reader may refer to reference [13] for a comprehensive survey and bibliography of thinning algorithms.

The second category is to compute the symmetric axes using *direct*, or *analytical* methods by approximating the object's boundary by a polygon. For noisy or biological (as cells) objects, this approximation leads to unavoidable inaccuracy. Algorithms belonging to this category are based on either heuristic methods [16, 17, 18] or more rigorous methods such as Vonoroi diagram [19, 20]. Although this category has many advantages over thinning algorithms (since they make measurements of Euclidean distance in the continuous domain rather than in the digital grid), they are of little practical use mainly because of their computational complexity (for example, the Vonoroi diagram).

The third category of skeletonization algorithms is the *ridge following* algorithms. From the object shape, the *Distance Transform* (DT) is obtained, from which ridges are found. The pro-

jection of these ridges constitute the skeletal branches of the object. Ridges can be traced by the active contour model [10] and by other methods [21]. Different DT's have been published in the literature. (See [10] for a survey). Algorithms in this category are relatively simple. In general, the skeletonization results of this category are more accurate and smoother than those of the other two categories [10]. A major drawback of algorithms in this category is that the DT of an object is sensitive to noise. Equidistance contours are as noisy as the boundary. Representative examples of this category can be found in references [22, 23].

A number of algorithms are based on the combination of different features from the aforementioned categories such as the Charge Particle Method (CPM), introduced in [27]. The CPM considers the object pixels of a binary image as particles with the same charge magnitude and the same charge polarity. The concept of the force of attraction or repulsion between charged particles is used in this algorithm for skeleton generation.

The proposed EFT-based approach has some commonalities with algorithms in the ridge following category, where the DT is replaced by an *electrostatic potential surface transform* and the ridge following process by the tracing of field lines passing through significant convexities and concavities detected along some equipotential contour. The proposed potential surface approach can represent the object's shape at different levels of smoothing or scale and can capture important shape information such as curvature. Furthermore, equipotential contours are smoother than equidistance contours which are employed in the ridge following category.

3 Electrostatic Field-Based Approach to Skeletonization

The various skeletonization algorithms developed use the binary image of an object as the input. The input to the presented skeletonization algorithm is a binary image of the boundary of an object. For example, the input to the EFT-based approach can be the edges of the object detected by an edge-detector. In the EFT-based method the boundary points are modeled as unit charges, and their values are set to 1 (see Figure 1).

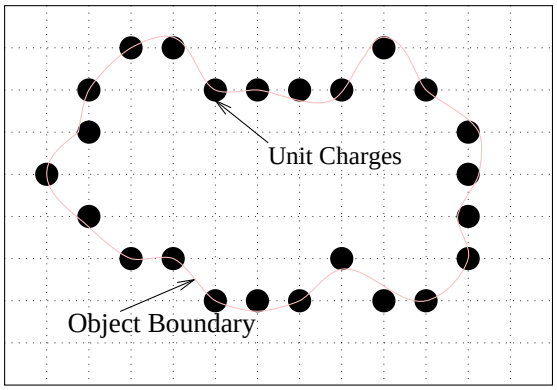

Figure 1: The model of the problem to generate the potential distribution on the object boundary.

In the proposed approach, a skeleton is defined as following:

$$S = \{(x, y) \mid E(x, y) \text{ is a local maximum or minimum or } v(x, y) = 0\},$$

where $v(x, y)$ is the potential at the location (x,y) inside the object, and $E(x, y) = |\nabla v(x, y)|$ is the electrostatic field of the object. S represents the electrostatic field lines passing through points of significant convexities and concavities, and the points of zero potential. This definition differs from the conventional definition of a skeleton.

The following are the steps required to find the skeleton of a planar object:

1. Compute the potential distribution $V = v(x, y)$ inside the object,

2. Compute the electrostatic field in x and y directions: E_x and E_y, respectively,

3. Find the equipotential contour at a given potential v_{con},

4. Detect significant convexities and concavities along an equipotential contour, and

5. Trace skeletal points starting from points of significant convexities and concavities,

The following subsections give details of each of the above steps.

3.1 Solution of the Potential Distribution Inside the Object

The presented method of computation of the potential distribution inside the object uses a predefined structuring element. The structuring element K is as large as the image. The value of the element at location (x, y) is $\frac{1}{\sqrt{(x^2+y^2)}}$. It gives the contribution of a unit charge located at that location because the electrostatic potential $v(x, y)$ at the center is inversely proportional to the distance between (x, y) and the center of the mask. Hence, the total potential at the center of the mask is the summation of all the potentials due to charges within the neighborhood of the mask. The potential distribution is given by the convolution of K with the input image, which can be computed efficiently using the Fast Fourier Transform (FFT). The FFT of K is computed and then it is pointwise multiplied with the FFT of the input image. The inverse FFT is then performed to obtain the potential field distribution of the image.

After the potential distribution is computed, it is normalized as follows. The maximum potential of the object boundary is set equal to 255 and the minimum potential is set equal to 0. The potential values inside the object are computed using a simple linear transformation. The potential outside the object is set equal to 255.

The normalized map $V = v(x, y)$ is the potential surface of the object that is utilized for the

construction of the skeleton. Figure 2 illustrates the potential surface generated for the image of a maple leaf.

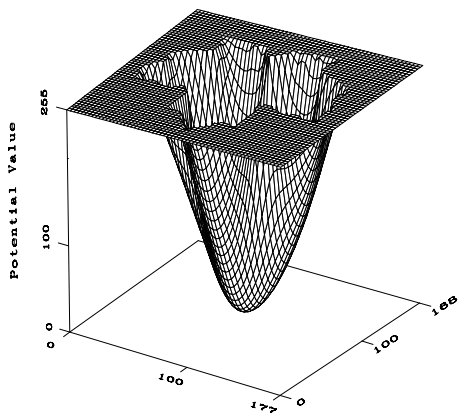

Figure 2: The potential surface generated for the image of a maple leaf.

3.2 Solution of the Electrostatic Field of the Object

The proposed approach for skeleton tracing uses the electrostatic field computed in x and y directions: E_x, and E_y, respectively. The computation for E_x, and E_y uses two structuring elements M_x and M_y. One for the x-direction, and one for the y-direction. The entries for the x-direction mask M_x are $-\frac{x}{r^3}$, where r is the distance from the center of the mask, similarly for the y-direction mask M_y the entries are $-\frac{y}{r^3}$. The electrostatic field in x-direction and y-direction is given by a convolution with M_x mask and M_y mask, respectively. The computation of E_x, and E_y is done using the FFT, similar to that for the computation of the potential distribution.

3.3 Construction of an Equipotential Contour at a Given Potential

The equipotential contour is used to detect significant convexities and concavities along the contour from which skeletal branches are initiated. This step can be visualized as a potential surface $V = v(x, y)$ being cut by a constant potential plane (parallel to the x-y plane). The curve that results from the intersection of the potential surface and the cutting plane is a closed contour.

The construction of a connected equipotential contour at a given potential, v_{con} within the range $0 - 255$, is based on the E_x, and E_y maps.

First, the starting point x_0, y_0 of the equipotential contour, at which the potential is equal to v_{con}, is detected. Starting from this point, the equipotential contour is built at the subpixel resolution. It is well known that the equipotential contour is perpendicular to the field lines. Therefore the tracing direction of the contour is perpendicular to that given by the direction of the electrostatic field, which is specified by $E_x(x, y)$ and $E_y(x, y)$ values. Thus, the next point (x_n, y_n) of the equipotential contour is chosen as following:

$$x_n = x_{n-1} - E_y(x_{n-1}, y_{n-1}) \times \delta,$$

$$y_n = y_{n-1} + E_x(x_{n-1}, y_{n-1}) \times \delta,$$

where $E_x(x, y)$ and $E_y(x, y)$ are the electrostatic field values in x and y-directions at (x, y) location, respectively, and δ is the step size. In the implementation, δ is chosen to be 1 for all experiments. The result of this step is one-dimensional curve $E(s)$ at the given potential v_{con}.

It is worth noting that the lower the value of the contour potential v_{con}, the smoother is the contour, the less the number of extrema of the field, and the less the number of significant convexities and concavities. This is expected due to the smoothing effect of the solution of the potential distribution inside the object.

From the above discussion, it is evident that the proposed skeletonization approach has the advantage of a multiscale approach. By appropriately choosing the equipotential contour at potential v_{con}, the desired level of details (or scale) of the skeleton can be selected. In particular, choosing an equipotential with a low value of v_{con}, a coarse skeleton is generated, whereas choosing an equipotential with a high value of v_{con}, a fine skeleton is generated. Such a smoothing effect has been used previously in reconstructing the three-dimensional default shape of an object from its occluding contour [33]. Figure 3 shows this interesting property of the potential distribution by depicting some equipotential contours of the maple leaf at various potentials.

Figure 3: Smoothing effect and multiscale property of equipotential contours of the maple leaf. The bright contour is the boundary. The gray contours are the equipotential contours. The equipotential contours shown are constructed in the potential range 5-180 in steps of 15. When the contour is closer to the center of the object, the contour gets smoother and details tend to disappear.

3.4 Detecting Corners along the Equipotential Contour

Starting from the field distribution $E(s)$ along the contour s, convex (concave) corners are located by identifying points having local minima (maxima) of the field $E(s)$. As mentioned in the previous step, the choice of the contour potential v_{con} directly determines the degree of detail of the skeleton.

Figure 4 demonstrates this fact by depicting different equipotential contours and their associated detected corners. The lower is the potential, the lower the number of corners detected. It should be noted that the interaction corner models discussed in reference [34], namely, the Γ, the *End*, and the *Stair* models, are also apparent in the EFT-based approach [11] and can be observed in Figure 4. For example, corners merging, disappearing, attracting, and repelling can be seen in the figure.

Figure 4: The equipotential contours and their associated corners (bright dots) of the maple leaf. The contours are constructed for the potential range 5-190 steps of 15. Notice that the number of corners increase with the potential v_{con}.

In this paper, both convex and concave corners are employed in generating skeletal branches. Many skeletonization algorithms consider only convex corners (e.g. [14]). Considering only convexities may be justified in certain applications as in the identification of pseudopods [14], but, both convexities and concavities must be considered because both contribute equally to the shape of an object. For a unique skeleton representation (see Section 2), both convexities and concavities must be considered (see Figure 5).

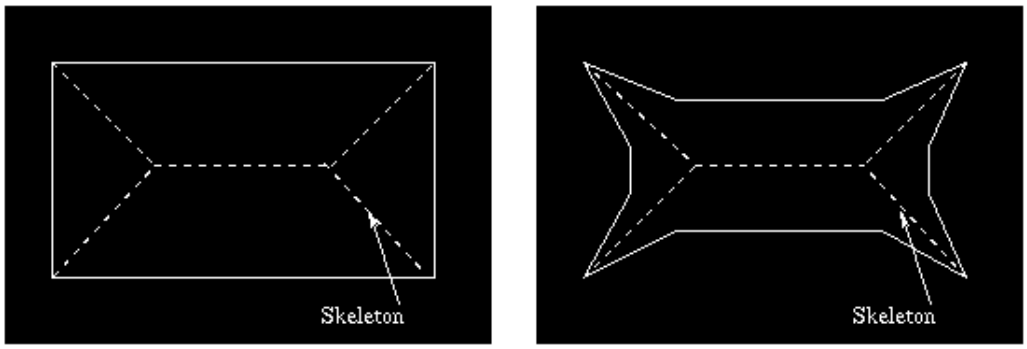

Figure 5: The same skeleton for different shapes. Considering only convexities and disregarding concavities leads to non-unique skeleton representation.

3.5 Skeleton Tracing

Having identified points of significant convexities and concavities along an equipotential contour at a potential v_{con}, these points are used to initiate the skeleton tracing procedure. The skeleton branches correspond to field lines passing through significant corners identified in the previous step. Therefore, the skeleton generation procedure is reduced to the problem of tracing the field lines.

Starting from the points having significant convexities and concavities along an equipotential contour of potential v_{con}, the field lines are traced in two directions: in the inward direction (downhill generation) towards the object's central region or pixel, in the potential range $v_c = 0$, and in the outward direction (uphill generation) towards the object's boundary, in the potential range $v_b = 255$. Tracing is done in the direction defined by $E_x(x, y)$, $E_y(x, y)$ values.

When tracing downhill the location of the next point x_n, y_n is defined at a subpixel resolution as following:

$$x_n = x_{n-1} - E_x(x_{n-1}, y_{n-1}) \times \delta,$$

$$y_n = y_{n-1} - E_y(x_{n-1}, y_{n-1}) \times \delta,$$

where $E_x(x, y)$ and $E_y(x, y)$ are the electrostatic field values in x and y-directions at (x, y) location,

respectively, and δ is the step size. In the implementation, δ is chosen to be 1. The tracing process in inward direction terminates when the object's central pixel or region at zero potential is reached, thus reaching its global minimum potential.

The same process is used for the uphill generation towards the object's boundary. This process is terminated when the object's boundary is reached, i.e. reaching its global maximum energy.

It is noteworthy that the skeletal branches generated by this procedure is guaranteed to meet at the minimum potential region since the potential distribution decreases monotonically in the inward direction up to the potential. Also the connectivity requirement of the skeleton is guaranteed using this approach because the electrostatic field lines must be continuous.

4 Experimental Results and Discussion

The EFT-based method allows the representation of the skeleton across a variety of scales. These multiscale skeletal representations can be obtained by changing the starting potential value for skeleton generation. At a finer scale (larger starting potential value), the skeleton has a large number of branches. At a coarser scale (lower starting potential value), the skeleton has fewer branches. Figure 6 clearly demonstrates this multiscale capability of the EFT-based approach. The skeleton generated at a potential of 90 (Figure 6a) is finer in scale and hence, has a larger number of branches when compared to that generated at a potential of 60 (Figure 6b).

A number of experiments were conducted using both synthesized and real images. We present the experimental results obtained by the EFT-based approach, a skeletonization algorithm based on the Euclidean Distance Transform [25] and the Charge Particle Method [27]. Figure 7 illustrates skeletons generated for a noise-free image using these techniques.

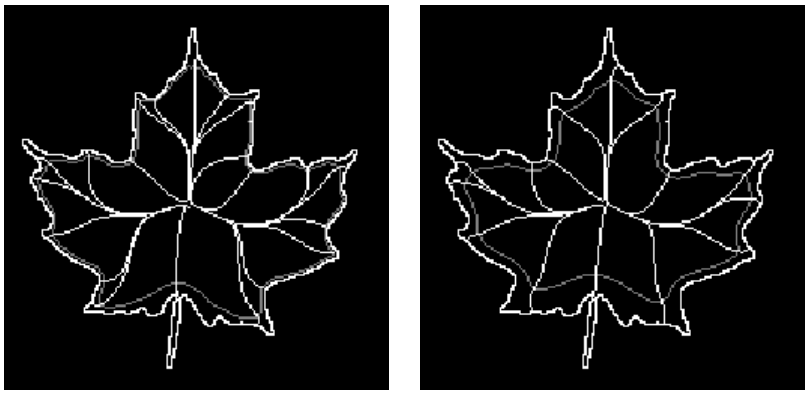

(a) (b)

Figure 6: The multiscale capability of the proposed approach. Skeletons generated for a maple leaf at two different starting equipotentials: (a) 90, and (b) 60.

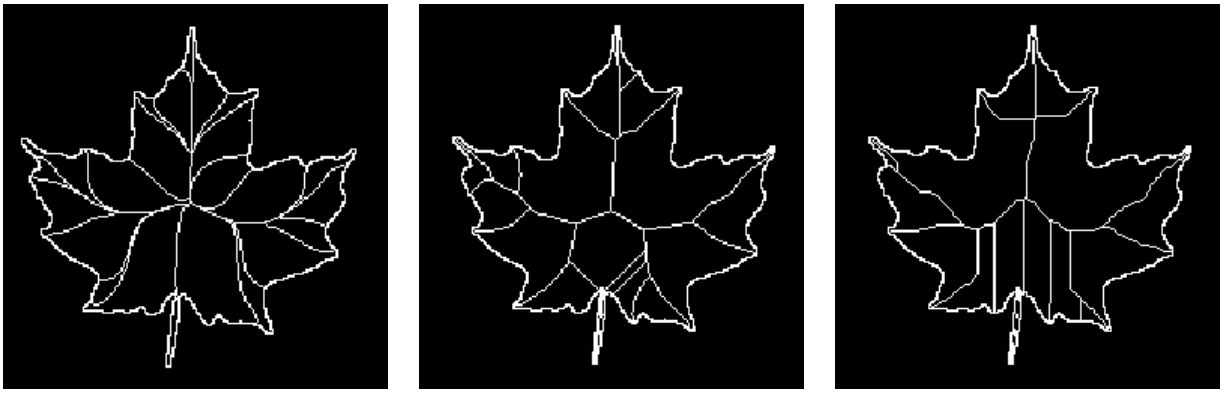

(a) (b) (c)

Figure 7: Skeletons generated for the image of a maple leaf. (a) EFT-based approach. Skeleton started at the equipotential contour 80; (b) DT-based algorithm; (c) Charge Particle Method.

To test the noise sensitivity, the boundary of the object is perturbed in the x and y directions by varying degrees of zero-mean Gaussian noise. The standard deviation σ of the noise is varied in the range from 0 to 20.

Figure 8 shows the results of skeletonization for the maple leaf image with boundary corrupted with noise of level $\sigma = 4$. Figure 9 illustrates the results for $\sigma = 10$ noise level. One can clearly see that the skeleton generated by the EFT-based approach is insensitive to the presence of boundary noise, whereas the skeletons generated by both the Euclidean distance algorithm and the Charge

Particle Method are very sensitive to the presence of boundary noise.

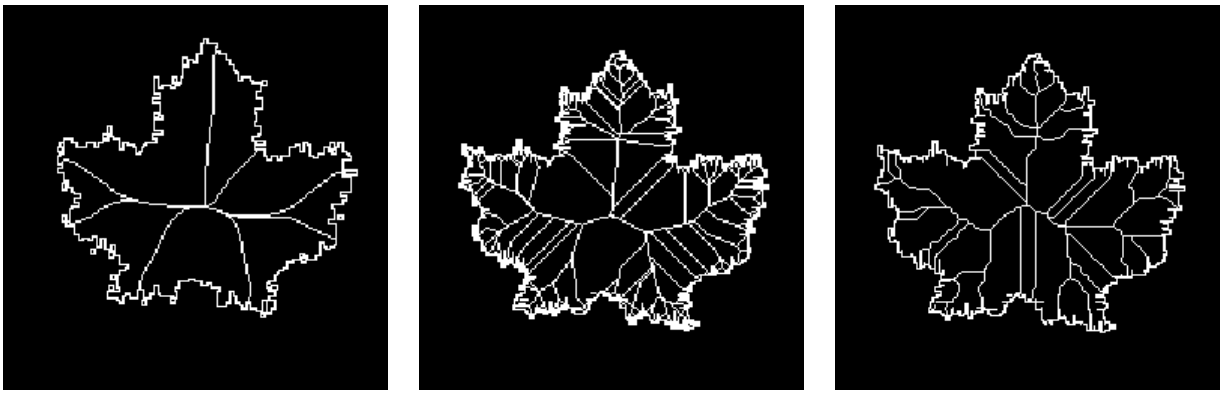

(a) (b) (c)

Figure 8: Skeletons generated for the image of a maple leaf with boundary corrupted with noise of level $\sigma = 4$. (a) EFT-based approach. Skeleton started at the equipotential contour 80; (b) DT-based algorithm; (c) Charge Particle Method.

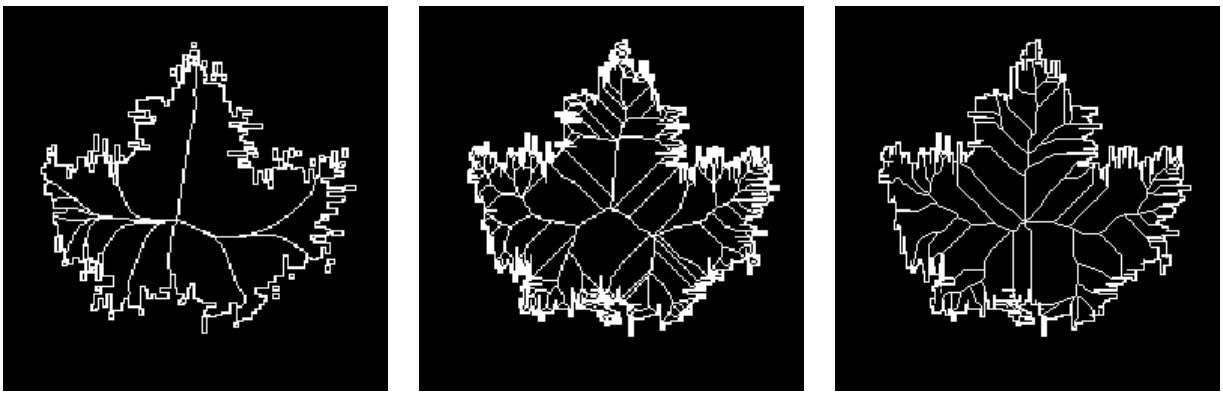

(a) (b) (c)

Figure 9: Skeletons generated for the image of a maple leaf with boundary corrupted with noise of level $\sigma = 10$. (a) EFT-based approach. Skeleton started at the equipotential contour 80; (b) DT-based algorithm; (c) Charge Particle Method.

The experimental results for the image of a rectangle are demonstrated in Figures 10- 11. The boundary of the original image is corrupted with noise of level $\sigma = 4$. Analysing the presented results, one can see that the EFT-based is less sensitive to boundary noise than both the Euclidean DT-based method and the Charge Particle Method.

The Charge Particle Method for the noise-free image of a rectangle produces a different skeleton

than expected. This can be explained by the nature of the CPM. The CPM models the object pixels of a binary image as charged particles. It assumes that the boundary of the object is maintained under higher potential than the particles. Therefore, the movement of the particles towards the medial axis is accomplished by the interaction of the electrostatic forces between individual particles and the entire boundary. In each pass the CPM deletes a set of edge points from the input. Each edge point is tested against the conditions for its removal. The process is repeated iteratively till particles attain a state of equilibrium at which the resulting force acting on them is zero. For objects such as a rectangle, ellipse, all conditions of the CPM for particles removal are satisfied, because the CPM assumes that the resultant force acting on a certain particle is due to the cumulative effect of eight immediate neighboring particles. This restriction was proposed based on the observation that the force acting between particles is inversely proportional to the square of the distance between them [27]. At each iteration all edge points for such type of images are removed, resulting in incorrect thinning of the pattern.

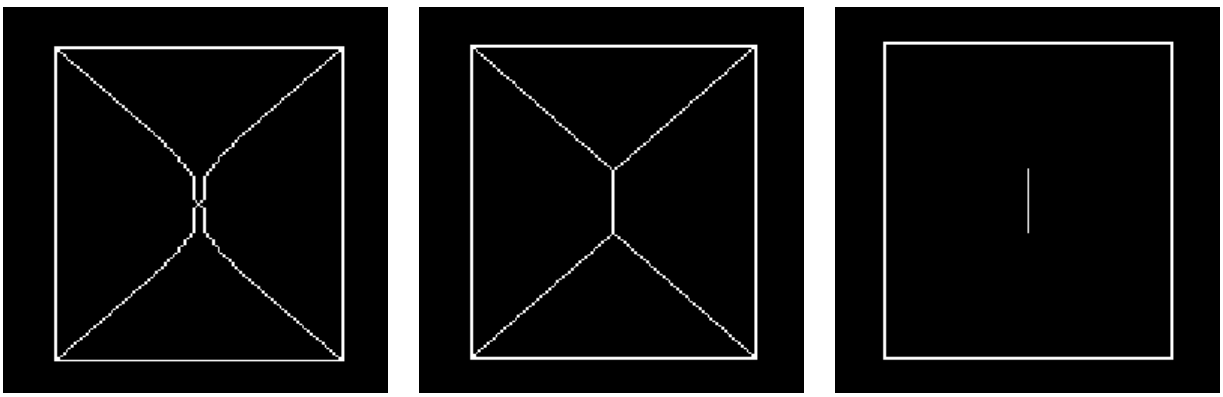

(a) (b) (c)

Figure 10: Skeletons generated from the image of a rectangle. (a) EFT-based approach. Skeleton started at equipotential contour 180; (b) DT-based method; (c) Charge Particle Method.

The above described skeletonization techniques were tested on a DEC alpha running OSF/1 V3.0. The EFT-based, DT-based, and CPM algorithms are written in the C programming lan-

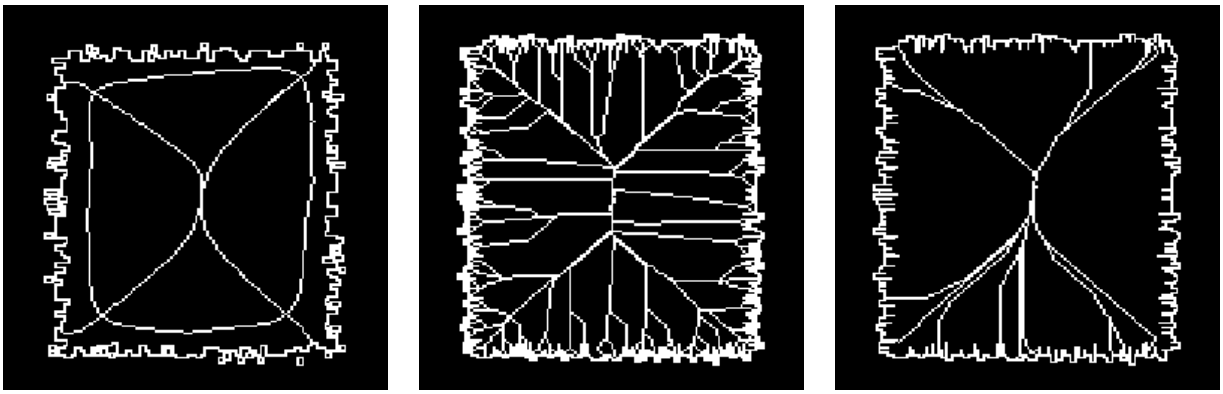

(a) (b) (c)

Figure 11: Skeletons generated from the image of a rectangle with boundary corrupted with a noise of level $\sigma = 4$. a) EFT-based approach. Skeleton started at equipotential contour 140; (b) DT-based algorithm; (c) Charge Particle Method.

guage. Tools in the Cantata visual programming environments were also employed [45]. In [27], it was pointed out that the CPM is almost as fast as the DT-based approach. The proposed method also has the same order magnitude in performance as the other two methods. A more quantitave timing analysis is beyond the focus of this paper. The quantitative evaluation of performance in the presence of noise is presented in the following section.

5 Performance evaluation and analysis

The main objective of any thinning algorithm is to obtain a connected skeleton of unit width along the medial axis of a given pattern. The resulting skeleton should inherit all the topological features of the original image. The following characteristics are usually used to judge the quality of the resulting skeletons: connectivity, thinness, symmetry of the skeleton, and sensitivity to noise. Computational complexity of the skeletonization algorithm and its reconstruction abilities are also important characteristics considered in the literature.

The proposed algorithm may be run with the option that the resultant skeletal points are labeled with their distance values to the object's boundary. Therefore, the original object can almost completely be recovered by means of a reverse-distance transformation. The Euclidean distance values are computed only for the skeletal points. The Charge Particle Method and DT-based algorithm that are used in this paper also allow reconstruction of the original pattern, for example, by adopting the approach described in [30].

The connectivity and thinness requirements of the skeleton generated by the proposed approach are guaranteed, as explained above. Other thinning techniques do not always satisfy these requirements. Morphological thinning algorithm [31] does not give connected skeletons.

We evaluate the performance of the proposed skeletonization approach in the presence of noise using the Hausdorf distance measure [9, 28]. Given two sets A and B, the Hausdorf distance is defined by $\max \{ \inf \{r \mid A \subseteq B \oplus disk(r)\}, \inf \{r \mid B \subseteq A \oplus disk(r)\} \}$.

For each algorithm, in this experiment, the image of the rectangle was used. The image size is 256×256. The skeleton generated for a noise-free image is compared to that generated for images at different levels of boundary noise that varies in the range from 2 to 20. Figure 12 shows the variation of the Hausdorf distance measure versus the level of noise present in the input image for the skeletonization. As we can see that the EFT-based approach is less sensitive to noise in comparison with the DT-based approach and the Charge Particle Method.

In Section 4, we have seen the experimental results of skeletons of a rectangle with boundary corrupted with various noise level (Figures 10 - 11). It can be observed that the skeletons extracted by the proposed approach is quite insensitive to boundary noise. However, the Hausdorf distance does not fully reflect this fact. The maple leaf image was not employed because the number of branches in the skeletons varies with the noise level. As a result, the Hausdorf distance measure

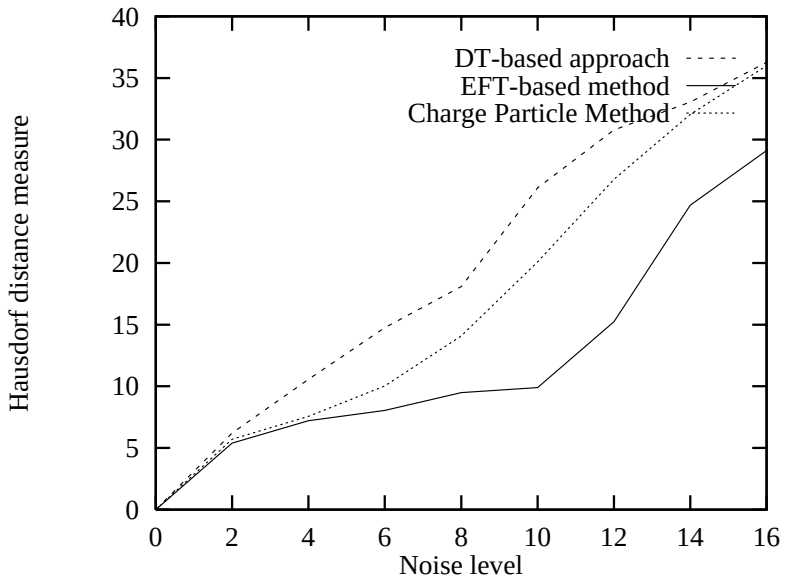

Figure 12: The Hausdorf distance measure between the skeleton for a noise-free image and the skeletons for the images with different levels of boundary noise.

is very high and does not appear to reflect the quality of the extracted skeletons. Much work is needed in the direction of skeleton evaluation.

6 Conclusions and Future Work

In this paper, a new approach for skeletonization that relies on the EFT has been presented. The details of the steps that constitute the proposed skeletonization approach have been described. The approach has been shown to possess a number of desirable features that can naturally solve many problems that have challenged existing skeletonization approaches. First, connectivity and thinness are guaranteed in the proposed approach. Secondly, the EFT approach gracefully captures and unifies notions of corner detection, multiscale representation, thinning, and skeletonization. Thirdly, the insensitivity of the proposed approach to severe boundary noise has been demonstrated experimentally. Moreover, since the new skeletonization approach is developed based on a well-

established theory, the electrostatic field theory, the performance of the proposed approach under varying conditions can be predicted and justified before experiments are even conducted.

The potential distribution in its own constitutes a useful representation of objects at various levels of details similar to the multiscale curvature-based shape representation approach [1], [2]. In the proposed approach, scale is naturally defined by the potential distribution. In fact, the equipotential contours generated from the potential surface can be viewed as fingerprints of the object [41] for robust representation and recognition, the application of which is an interesting research topic.

Experimentally we found that the Hausdorf distance measure does not fully reflect the experimental results obtained. Evaluation of skeletons is still an open issue.

The extension of EFT-based approach for shapes with holes is beyond the study of this paper. In order to extend this model to work for images with holes we can model the boundaries of the object with different potential values, e.g positive charges to the outer boundary and negative charges to the boundaries of holes.

Our research work using the EFT framework for solving computer vision problems inspires further research using the same approach in addressing other vision problems. A natural extension to the EFT-based approach is to use it in representing multidimensional objects. The potential surface becomes the *potential volume* and the equipotential contours are replaced by equipotential surfaces. Also, the electrostatic field extrema would correspond to curvature extrema, and hence, three-dimensional edges and three-dimensional corners can be detected using the same methodology described in this paper. Once the potential volume is estimated, the three-dimensional skeleton of a three-dimensional object [21], [40], which has a special importance in biomedical applications, can be extracted. Another extension to the approach is to study the use of the EFT-based method

in segmentation.

The experience in this work suggests that interesting features exhibited by the electrostatic field-based approach of corner detection and skeletonization promote the investigation of more physics-based models in solving computer vision problems. Finally, it is believed that borrowing simple ideas from other disciplines, such as physics, will certainly benefit research in the computer vision community.

References

[1] F. Mokhtarian and A. K. Mackworth, Scale-based description and recognition of planar curves and two-dimensional shapes, *IEEE Transactions on Pattern Analysis and Machine Intelligence*, Vol. 8, No. 1, pp. 34-43, 1986.

[2] F. Mokhtarian and A. K. Mackworth, A theory of multiscale, curvature-based shape representation for planar curves, *IEEE Transactions on Pattern Analysis and Machine Intelligence*, Vol. 14, No. 8, pp. 789-805, 1992.

[3] H. Blum, A transformation for extracting new descriptors of shape, in *Models for the Perception of Speech and Visual Form* (W. Wathen-Dunn, ed.), Cambridge MA: MIT Press, 1967.

[4] R. W. Smith, Computer processing of line images: A survey, *Pattern Recognition*, Vol. 20, No. 1, pp. 7-15, 1987.

[5] R. M. Haralick, Performance characterization in image analysis: thinning, a case in point, *Pattern Recognition Letters*, Vol. 13, pp. 5-12, 1992.

[6] L. Lam and C. Y. Suen, Automatic evaluation of skeleton shapes, in *Proc. 11th Int. Conference on Pattern Recognition*, The Haque, The Netherlands, pp. 342-345, 1992.

[7] S.-W. Lee, L. Lam, and C. Y. Suen, Performance evaluation of skeletonization algorithms for document image processing, in *Proc. 1st Int. Conference on Document Analysis and Recognition*, St. Malo, France, pp. 260-271, 1991.

[8] R. Plamondon and C. Y. Suen, On the definition of reference skeletons for comparing thinning algorithms, in *Proc. Vision Interface 1988*, Edmonton, Canada, pp. 70-75, 1988.

[9] M. Y. Jaisimha, R. M. Haralick, A methodology for the characterization of the performance of thinning algorithms, in *ICDAR*, pp. 282-286, 1993.

[10] F. Leymarie and M. D. Levine, Simulating the grassfire transform using an active contour model, *IEEE Transactions on Pattern Analysis and Machine Intelligence*, Vol. 14, No. 1, pp. 56-75, 1992.

[11] G. H. Abdel-Hamid and Y. H. Yang, Electrostatic field-based detection of corners of planar curves, *Proceedings of the 1993 Canadian Conference on Electrical and Computer Engineering*, Vancouver, Canada, pp. 767-770, 1993.

[12] G. H. Abdel-Hamid and Y. H. Yang, Multiscale Skeletonization: An electrostatic field-based approach, *Proc. IEEE Int. Conference on Image Processing*, Austin, Texas, Vol. 1, pp. 949-953, Nov. 13-16, 1994.

[13] L. Lam, S.-W. Lee, and C. Y. Suen, Thinning methodologies - a comprehensive survey, *IEEE Transactions on Pattern Analysis and Machine Intelligence*, Vol. 14, No. 9, pp. 869-885, 1992.

[14] A. R. Dill, M. D. Levine, and P. B. Noble, Multiple resolution skeletons, *IEEE Transactions on Pattern Analysis and Machine Intelligence*, Vol. 9, pp. 495-504, 1987.

[15] Z. Guo and R. W. Hall, Fast fully parallel thinning algorithms, *CVGIP: Image Understanding*, Vol. 55, No. 3, pp. 317-328, 1992.

[16] C. Arcelli, Pattern thinning by contour tracing, *Computer Graphics Image Processing*, Vol. 17, pp. 130-144, 1981.

[17] M. P. Martinez-Perez, J. Jimenez, and J. L. Navalon, A thinning algorithm based on contours, *Computer Graphics and Image Processing*, Vol. 39, 1987, 186-201, 1987.

[18] B. Shapiro, J. Pisa, and J. Sklansky, Skeleton generation from x, y boundary sequences, *Computer Graphics and Image Processing*, Vol. 15, pp. 136-153, 1981.

[19] J. W. Brandt and V. R. Algazi, Continuous skeleton computation by Vonoroi diagram, *CVGIP: Image Understanding*, Vol. 55, No. 3, pp. 329-338, 1992.

[20] R. Ognriewicz and M. Ilg, Vonoroi skeletons: theory and applications, in *Proc. IEEE Conference on CVPR*, Champaign, Illinois, pp. 63-69, 1992.

[21] J. Gauch and S. Pizer, The intensity axis of symmetry and its application to image segmentation, *IEEE Transactions on Pattern Analysis and Machine Intelligence*, Vol. 15, No. 8, pp. 753-770, 1992.

[22] P. E. Danielsson, Euclidean distance mapping, *Computer Graphics and Image Processing*, Vol. 14, pp. 227-248, 1980.

[23] F. Klein and O. Kubler, Euclidean distance transformation and model guided image interpretation, *Pattern Recognition Letters*, Vol. 3, pp. 19-30, 1987.

[24] F. Y. Shin and O. R. Mitchell, A mathematical morphology approach to euclidean distance transformation, *IEEE Transactions on Image Processing*, Vol. 1, No. 2, pp. 197-204, 1992.

[25] F. Y. Shin and C. C. Pu, A skeletonization algorithm by maxima tracking on euclidean distance transform, *Pattern Recognition* , Vol. 28, No. 3, pp. 331-341, 1995.

[26] C. Arcelli and G. Sanniti di Baja, A width independent fast thinning algorithm, *IEEE Transactions on Pattern Analysis and Machine Intelligence*, Vol. 7, pp. 463-474, 1985.

[27] A. Arumugam, T. Radhakrishnan, and C. Y. Suen, A thinning algorithm based on the force between charged particles, *Int. Journal of Pattern Recognition and Artifitial Intelligence*, Vol. 7, No. 5, pp. 988-1008, 1993.

[28] R. M. Haralick, and L. G. Shapiro, Computer and Robot Vision, Addison-Wesley Inc. 1992

[29] D. P. Huttenlocher, G. A. Klanderman, and W. J. Ruckidge, Comparing Images Using the Hausdorff Distance, *IEEE Transactions Pattern and Analysis Machine Intelligence*, Vol. 15, No. 9, pp. 850-863, 1993.

[30] T. Pavlidis. An asynchronous thinning algorithm. *Computer Graphics and Image Processing*, No. 20, pp. 133-157, 1982.

[31] C. R. Giardina and E. Dougherty Morphological methods in image and signal processing, Prentice-Hall, 1988.

[32] G. Chen and Y. H. Yang, Edge detection by regularized cubic B-spline fitting,*IEEE Trans. Systems, Man and Cyber.*, Vol. 25, No. 4, pp. 636-643, 1995.

[33] O. E. Vega and Y. H. Yang, Default shape theory: with application to the computation of the direction of the light source, *CVGIP: Image Understanding*, Vol. 60, No. 3, pp. 285-299, 1994.

[34] A. Rattarangsi and R. T. Chin, Scale-based detection of corners of planar curves, *IEEE Transactions Pattern and Analysis Machine Intelligence*, Vol. 14, No. 4, pp. 430-449, 1992.

[35] A. J. B. Fuller, *Engineering Field Theory*, Pergamon Press, Oxford, 1973.

[36] B. K. P. Horn and M. J. Brooks, The variational approach to shape from shading, *Computer Vision, Graphics, and Image Processing*, Vol. 33, pp. 174-208, 1986.

[37] F. Leymarie, Tracking and describing deformable objects using active contour models, M. Sc. thesis, McGill University, Montreal, Quebec, Canada, 1990.

[38] A. R. Mitchell and D. F. Griffiths, *The Finite Difference Method in Partial Differential Equations*, John Wiley, 1980.

[39] R. Mittra and S. W. Lee, *Analytical Techniques in The Theory of Guided Waves*, McMillan, New York, pp. 4-11, 1971.

[40] T. Nguyen and J. Sklansky, Reconstructing the 3-D medical axes of coronary arteries in single-view cineangiograms, *IEEE Transactions on Medical Imaging*, Vol. 13, No. 1, pp. 61-73, 1994.

[41] M. A. Piech, Comment on fingerprints of two-dimensional edge models, *Computerj Vision, Graphics and Image Processing*, Vol. 42, pp. 381-386, 1988.

[42] T. Simchony, R. Chellappa, and M. Shao, Direct analytical methods for solving Poisson equations in computer vision problems, *IEEE Transactions Pattern Analysis and Machine Intelligence*, Vol. 12, No. 5, pp. 435-446, 1990.

[43] I. N. Sneddon, *Elements of Partial Differential Equations*, McGraw-Hill, New York, 1957.

[44] D. Terzopoulos, Image analysis using multigrid relaxation methods, *IEEE Transactions on Pattern Analysis and Machine Intelligence*, Vol. 8, pp. 129-139, 1986.

[45] Krohos Research Inc., 1994.